Oxygen Nonstoichiometry and Defect Chemistry Modeling of Ce0.8Pr0.2O2-delta

Chatzichristodoulou, Christodoulos; Hendriksen, Peter Vang

Published in:
Electrochemical Society. Journal

Link to article, DOI:
10.1149/1.3288241

Publication date:
2010

Document Version
Publisher's PDF, also known as Version of record

Journal of The Electrochemical Society, **157** (4) B481-B489 (2010)
0013-4651/2010/157(4)/B481/9/$28.00 © The Electrochemical Society

Oxygen Nonstoichiometry and Defect Chemistry Modeling of $Ce_{0.8}Pr_{0.2}O_{2-\delta}$

C. Chatzichristodoulou[a,b,z] **and P. V. Hendriksen**[a]

[a]*Fuel Cells and Solid State Chemistry Division, Risø DTU National Laboratory for Sustainable Energy, DK-4000 Roskilde, Denmark*
[b]*Niels Bohr Institute, University of Copenhagen, DK-2100 Copenhagen, Denmark*

The oxygen nonstoichiometry (δ) of $Ce_{0.8}Pr_{0.2}O_{2-\delta}$ has been measured as a function of P_{O_2} at temperatures between 600 and 900°C by coulometric titration and thermogravimetry. An ideal solution defect model, a regular solution model, and a defect association model, taking into account the association of reduced dopant species and oxygen vacancies, were unable to reproduce the experimental results. However, excellent agreement with the experimentally determined oxygen nonstoichiometry could be achieved when using either a nonideal solution model with an excess enthalpic term linear in δ ($\Delta H_{Pr}^{exc} = a_H\delta$) and a completely random distribution of defects (referred to as "δ-linear"), or a "generalized δ-linear" solution model, where the excess Gibbs energy change in the reduction reaction of the dopant linearly varies with δ ($\Delta G_{Pr}^{exc} = a_G\delta$). A comparison of the partial molar enthalpy and entropy of oxidation, estimated from the defect models with those determined directly from the oxygen nonstoichiometry, suggests that the δ-linear solution model is the most appropriate in accounting for the observed nonideal reduction behavior of Pr.
 [DOI: 10.1149/1.3288241]

Manuscript submitted July 7, 2009; revised manuscript received December 8, 2009. Published February 9, 2010.

Ceria-based mixed oxides have been extensively studied as their properties can be tailored by appropriate doping to match the requirements of a variety of applications, such as electrolytes and electrodes for solid oxide fuel cells,[1] three-way catalysts,[2] oxygen sensors,[3] and oxygen permeation membranes.[4]

The oxygen nonstoichiometry (δ) of pure and doped ceria increases with decreasing oxygen partial pressure and increasing temperature, accompanied by the partial reduction of Ce^{4+} to Ce^{3+}. The partial molar enthalpy for oxygen incorporation ($h_O - h_O^o$) of pure ceria strongly depends on δ.[5,6] The absolute value of $h_O - h_O^o$ rapidly decreases up to $\delta \approx 0.1$ and goes through a minimum at $\delta \approx 0.15$.[5,6] The δ dependence of $h_O - h_O^o$ was less pronounced for δ between 0.1 and 0.25.[5,6] The absolute value of $h_O - h_O^o$ in ceria doped with 10 atom % Gd also rapidly decreases up to a total oxygen vacancy concentration of ~0.12.[7] For $Ce_{0.8}Gd_{0.2}O_{1.9-\delta}$, where the total oxygen vacancy concentration at oxidizing conditions is already 0.1, no clear δ dependence of $h_O - h_O^o$ could be observed.[8] Despite the strong δ dependence of $h_O - h_O^o$, the absolute value of $h_O - h_O^o$ is only slightly affected by the degree of doping, when the values are compared at the same total oxygen vacancy concentration (or at the same concentration of trivalent cations).[9]

Examples of nonideal behavior with δ-dependent $h_O - h_O^o$ have been reported for other oxide systems as well. A regular solution behavior (which for small δ corresponds to a linear dependence of $h_O - h_O^o$ on δ) has been observed for the reduction of the perovskite compounds $La_{1-x}Sr_xCrO_{3-\delta}$[10] and $La_{1-x}Sr_xCoO_{3-\delta}$.[11] In both cases, the partial molar enthalpy of oxidation linearly decreases with increasing oxygen nonstoichiometry. A generalization of the regular solution model has been proposed, allowing for a δ dependence of the excess free energy (ΔG^{exc}) because an excess entropic term that varies with oxygen nonstoichiometry may also exist.[12] Furthermore, for $La_{1-x}Ca_xCrO_{3-\delta}$, a linear relationship should be expected between the excess Gibbs energy change (ΔG^{exc}) and δ based on the estimation of pair potential changes due to the defect-induced lattice expansion.[12] A significant deviation from ideality has also been observed for the redox energetics of $SrFeO_{3-\delta}$.[13] For this material, a regular solution model was unable to account for the deviation from ideality, which, however, could be successfully interpreted by a nonideal model with an excess term of a purely configurational entropic origin.[13]

[z] E-mail: ccha@risoe.dtu.dk

When doping CeO_2 with Pr, a change in the oxygen nonstoichiometry with varying oxygen activity is expected in the high P_{O_2} range, corresponding to the reduction of Pr, as well as at low P_{O_2} values, corresponding to the reduction of Ce. Some discrepancies exist in the literature on the solubility limit of Pr in CeO_2. A solubility limit of 30 atom %, as determined by X-ray diffraction (XRD), was reported by Shuk and Greenblatt[14] and Ftikos et al.[15] In contradiction to this, single-phase fluorite samples with Pr doping up to 55 atom %[16] or even 70 atom % were reported by Knauth and Tuller[17] and Rajendran et al.[18] The oxygen nonstoichiometry of 20 atom % Pr-doped ceria has been investigated in the high P_{O_2} regime (10^{-5}–10^{-1} atm) in the temperature ranges of 800–950°C (for microcrystalline powder)[19] and 600–750°C (for nanocrystalline powder)[20] by coulometric titration (CT). In both cases, a simple defect model treating the reduction of Pr^{4+} to Pr^{3+} in an ideal manner (i.e., not allowing $h_O - h_O^o$ to vary with the degree of nonstoichiometry) accounted well for the determined nonstoichiometry data.

Here, the oxygen nonstoichiometry of $Ce_{0.8}Pr_{0.2}O_{2-\delta}$ is reported (for microcrystalline powder, $D_{particle} \sim 1$ to 5 μm), as determined by CT and thermogravimetry (TG), over a wide P_{O_2} range, covering both the reduction of Pr and Ce at temperatures between 600 and 900°C. Five defect models have been considered to analyze the experimental data.

1. Ideal model: ideal reduction of both Ce and Pr (i.e., constant standard enthalpy, ΔH^o, and entropy, ΔS^o, of the reduction reaction and random distribution of defects).
2. Association model: ideal reduction of Ce and Pr, but defect interaction among reduced Pr and oxygen vacancies is assumed, leading to the formation of singly charged defect associates.
3. Regular model: ideal reduction of Ce and regular solution behavior[21] for Pr (i.e., $\Delta H_{Pr}^o = \Delta H_{Pr,\delta=0}^o + x_{Ce_{0.8}Pr_{0.2}O_2} x_{Ce_{0.8}Pr_{0.2}O_{1.9}} \Omega$, ΔS_{Pr}^o = const, and randomly distributed defects; Ω represents the magnitude of the deviation from the ideal solution).
4. Nonideal (δ-linear) model: ideal reduction of Ce and linear δ dependence of the excess enthalpic term for the reduction of Pr [i.e., $\Delta H_{Pr}^o = \Delta H_{Pr,\delta=0}^o + a_H\delta$, ΔS_{Pr}^o = const, and randomly distributed defects; a_H represents the rate of change in the partial molar enthalpy for the reduction of Pr with oxygen nonstoichiometry, $(d\Delta H_{Pr}^o)/d\delta$].
5. Generalized δ-linear model: ideal reduction of Ce and linear δ dependence of the excess free energy for the reduction of Pr (i.e.,

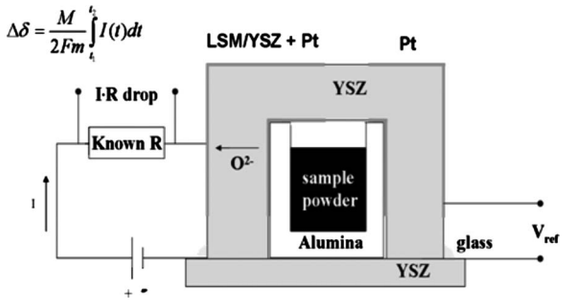

Figure 1. Experimental setup used for CT.

$\Delta G^{o}_{Pr} = \Delta G^{o}_{Pr} + a_G\delta$; a_G describes the deviation from the standard Gibbs energy change for the reduction of Pr).

The ability of each defect model to reproduce the experimental $\delta(\log P_{O_2})$ curves is examined, and the thermodynamic parameters estimated from the different defect models are compared to values directly determined from the oxygen nonstoichiometry data.

Experimental

Sample preparation and phase analysis.— $Ce_{0.8}Pr_{0.2}O_{2-\delta}$ powder was synthesized by coprecipitation. Aqueous solutions of $Ce(NO_3)_3{\cdot}6H_2O$ (Alfa Aesar, 99.99%) and $Pr(NO_3)_3{\cdot}xH_2O$ (Alfa Aesar, 99.9%) were prepared. The solution concentrations were measured both gravimetrically and by titration. Appropriate amounts of each solution were mixed with ~400 mL distilled/filtered water in a glass container at 200°C. Oxalic acid (1 M) was added while stirring the solution to achieve coprecipitation of the metal oxalates. The solution was dried overnight at 300°C, and the resulting powder was calcined at 600°C. The powder was shaped into disks at a uniaxial pressure of 3 MPa and further isostatically compressed in an evacuated latex container suspended in water at a pressure of 325 MPa. The disks were sintered at 1500°C in air for 12 h and slowly cooled to room temperature at a rate of 0.5 K/min. Phase analysis was performed by room-temperature XRD using a Bruker D8 Advance diffractometer with Cu Kα radiation and a LynxEye position sensitive detector. The $Ce_{0.8}Pr_{0.2}O_{2-\delta}$ powder was a single fluorite phase after sintering at 1500°C in air. A grain size in the range of 1–5 μm was determined by scanning electron microscopy (Zeiss Supra 35).

CT and TG.— Sintered disks were crushed into powders, examined for phase purity by XRD, and used for CT and TG. A schematic of the experimental setup used for CT is shown in Fig. 1. A small alumina cup with a known mass of sample powder (~2 g) was fitted in a $Zr_{0.85}Y_{0.15}O_2$ (YSZ) cup covered with a YSZ lid and sealed with glass (MgO/sodium aluminosilicate glass composite, 30/70 vol %) at 1000°C. The contact surfaces between the YSZ cup and the lid were polished using SiC paper and 3 μm diamond paste, and external uniaxial pressure was applied to the system to ensure a good seal. Four electrodes (two at the inner surface and two at the outer surface of the YSZ cup) served as working electrodes for electrochemical pumping of oxygen and reference electrodes for the determination of P_{O_2} inside the cup. Pt paste was used for the reference electrodes, whereas a thin (~10 μm) sprayed layer of YSZ/$La_{0.8}Sr_{0.2}MnO_3$ (LSM) cermet covered with Pt paste was used for the working electrodes. Integration of the current passing through the working electrodes over time yielded, by application of Faraday's law, the total amount of oxygen removed from the sample powder.

The leak rate of oxygen through the glass seal and/or cup porosity, $[(d\Delta\delta)/dt]_{leak}$, was determined in three ways.

A. The $[(dP_{O_2})/dt]_{empty}$ of an empty titration cell (no sample) was measured at various P_{O_2} values and temperatures over an extended period of time. The pressure was transformed to the number of moles (n_{O_2}) using the ideal gas law, $[(dn_{O_2})/dt]_{empty}$, and finally expressed as $[(d\Delta\delta)/dt]_{leak}$, assuming that the change in oxygen content originates from a change in δ of an equal amount of sample as in the filled cup. The leak rate estimated in this way was of the order of 10^{-32}, 10^{-19}, and 10^{-9} s^{-1} at 600, 700, and 800°C, respectively, indicative of a very good seal.

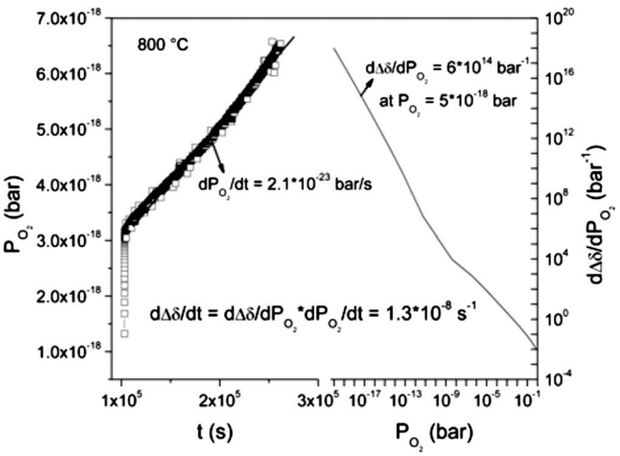

Figure 2. Estimation of the leak rate at 800°C at $P_{O_2} \sim 5 \times 10^{-18}$ bar using method C. The time dependence of the P_{O_2} in the titration cell after the oxygen pumping step is shown on the left and the P_{O_2} dependence of $[(d\Delta\delta)/dP_{O_2}]_{filled}$ is shown on the right.

B. The difference in pumped charge over an isothermal CT cycle was determined, and a mean leak rate was obtained from

$$\overline{\left(\frac{d\Delta\delta}{dt}\right)}_{leak} = \frac{Q_{out} - Q_{in}}{2Fnt} \quad [1]$$

where Q_{out} is the total charge needed to be pumped to reach the lowest P_{O_2} value of the titration cycle, Q_{in} is the total charge that has to be pumped to return to the starting point in P_{O_2}, n is the amount of powder in the titration cell expressed in moles, and t is the duration of the titration cycle. The advantage of this method is that the estimated leak rate is for the specific titration cell. Leak rates determined by this method were of the order of 10^{-10}–10^{-8} s^{-1} between 600 and 900°C.

C. The $[(dP_{O_2})/dt]_{filled}$ of the filled titration cell was measured at steady state, and the leak rates were estimated from

$$\left(\frac{d\Delta\delta}{dt}\right)_{leak} = \left(\frac{dP_{O_2}}{dt}\right)_{filled}\left(\frac{d\Delta\delta}{dP_{O_2}}\right)_{filled} \quad [2]$$

This approach allowed us to estimate the variation in the leak rate over time. The estimation of the leak rate with this method at 800°C at $P_{O_2} \sim 5 \times 10^{-18}$ bar is shown in Fig. 2. After equilibration, the rate of change in P_{O_2} in the titration cell is approximately constant and equal to 2.1×10^{-23} bar/s. By differentiating the $\Delta\delta(P_{O_2})$ plot, we find that the slope $[(d\Delta\delta)/dP_{O_2}]_{filled}$ at 800°C at $P_{O_2} \sim 5 \times 10^{-18}$ bar is 6×10^{14} bar^{-1}. Therefore, the leak rate for this specific titration cell at 800°C at $P_{O_2} \sim 5 \times 10^{-18}$ bar is estimated to be 1.3×10^{-8} s^{-1}. The leak rates determined in this manner were practically identical to the mean leak rates obtained by method B without a significant variation over time.

From the three estimates of the leak rates, it can be concluded that the relative error introduced in the measurement of δ by gas leaks, $[d(\Delta\delta/\delta)]/dt$, is of the order of 10^{-8} s^{-1}, and thus the titration cells could be allowed to equilibrate over extended periods of time without introduction of a significant error. The measured values of δ have been corrected for the determined leakages, and the magnitude

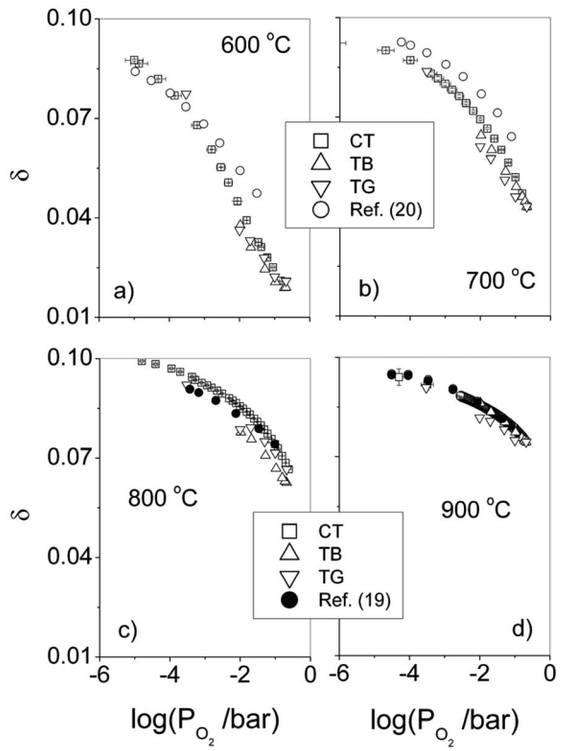

Figure 3. The oxygen partial pressure dependence of the oxygen nonstoichiometry determined at (a) 600, (b) 700, (c) 800, and (d) 900°C by CT, TG, and TB in the current investigation is compared to literature data.[19,20]

of the correction is taken as an uncertainty estimate (the experimental uncertainty of δ, as indicated in the plots, is twice the magnitude of this correction). The variation in the oxygen nonstoichiometry of LSM and of the oxygen content of the gas present in the dead volume of the cup are estimated to contribute by less than 0.1% of the measured change in δ in the P_{O_2} range related to the reduction of Pr and have therefore been neglected. However, in the P_{O_2} range related to the reduction of Ce, decomposition of the inner LSM working electrode may be expected.[22,23] This (assuming full decomposition of the LSM) gives rise to an error contribution of less than 10% of the change in oxygen nonstoichiometry Δδ. This potential error has been taken into account in the depicted uncertainty estimates along with the error due to leakages.

TG was performed using both a Netzsch STA 409CD thermogravimeter and a Netzsch TG 439 thermobalance (TB). The P_{O_2} of the sample atmosphere was varied by appropriate gas mixtures at constant temperature and measured with the help of a YSZ P_{O_2} sensor connected downstream. An equilibration time of 2 h was allowed after each gas change. This duration is expected to be more than adequate because the time constant for the relaxation, which may be estimated from the relation $\tau \sim L^2/D_{chem}$, is $\tau \sim 10^{-3}$ s using a value of $D_{chem} \sim 1 \times 10^{-5}$ cm^2/s for the chemical diffusion coefficient[24,25] and $L \sim 1$ μm for the grain size. The weight loss, measured with the thermogravimeter, was corrected for buoyancy effects using an alumina powder reference sample of the same volume, measured under identical conditions.

Results and Discussion

The oxygen nonstoichiometry of $Ce_{0.8}Pr_{0.2}O_{2-\delta}$, measured by CT, TB, and TG as a function of P_{O_2} at 600, 700, 800, and 900°C, is shown in Fig. 3a-d, respectively. Literature values are shown for comparison.[19,20] In Ref. 19, the change in oxygen nonstoichiometry Δδ is reported as a function of oxygen partial pressure with respect to air. To compare with our data, the $\Delta\delta(P_{O_2})$ values of Ref. 19 have been transformed to $\delta(P_{O_2})$ by shifting them by a constant to match with the δ value of the present study at the highest P_{O_2} reported in Ref. 19. Good agreement is observed between the oxygen nonstoichiometry data determined in the present study and those of Ref. 19 at 800 and 900°C, the difference being within the scattering observed for the present data determined by CT, TB, and TG. The oxygen nonstoichiometry reported for $Ce_{0.8}Pr_{0.2}O_{2-\delta}$ [20] at 700 and at 600°C in the P_{O_2} range 10^{-1}–10^{-3} bar is somewhat higher than the one determined in the current study. The discrepancy at 700°C might be due to the errors in the determination of the absolute value of δ. At 600°C though, the reported P_{O_2} dependence of δ shows a different behavior from our data, where oxidation appears sooner with increasing P_{O_2}. This difference is most likely because nanosized powder was used in Ref. 20, which facilitates the loss of oxygen.[26,27]

Five defect models were considered in the analysis of the measured oxygen nonstoichiometry at varying P_{O_2}.

1. Ideal model: The reduction of Pr and Ce is treated in an ideal manner (ΔH^o and ΔS^o independent of δ). The defect formation reactions and equilibrium constants read

$$O_O^x + 2Pr_{Ce}^x \leftrightarrow \tfrac{1}{2}O_2(g) + V_O^{\bullet\bullet} + 2Pr_{Ce}'$$

$$K_{Pr} = \exp\left(-\frac{\Delta H_{Pr}^o - T\Delta S_{Pr}^o}{RT}\right) = \frac{P_{O_2}^{1/2}[V_O^{\bullet\bullet}][Pr_{Ce}']^2}{[O_O^x][Pr_{Ce}^x]^2},$$

$$\Delta H_{Pr}^o, \Delta S_{Pr}^o = \text{const} \quad [3]$$

$$O_O^x + 2Ce_{Ce}^x \leftrightarrow \tfrac{1}{2}O_2(g) + V_O^{\bullet\bullet} + 2Ce_{Ce}'$$

$$K_{Ce} = \exp\left(-\frac{\Delta H_{Ce}^o - T\Delta S_{Ce}^o}{RT}\right) = \frac{P_{O_2}^{1/2}[V_O^{\bullet\bullet}][Ce_{Ce}']^2}{[O_O^x][Ce_{Ce}^x]^2},$$

$$\Delta H_{Ce}^o, \Delta S_{Ce}^o = \text{const} \quad [4]$$

The mass, site, and charge conservation conditions for this case are

$$[Pr_{Ce}^x] + [Pr_{Ce}'] = 0.2 \quad [5]$$

$$[Ce_{Ce}^x] + [Ce_{Ce}'] + [Pr_{Ce}^x] + [Pr_{Ce}'] = 1 \quad [6]$$

$$[O_O^x] + [V_O^{\bullet\bullet}] = 2 \quad [7]$$

$$2[V_O^{\bullet\bullet}] = [Pr_{Ce}'] + [Ce_{Ce}'] \quad [8]$$

$\Delta G_{Pr}^o = \Delta H_{Pr}^o - T\Delta S_{Pr}^o$ and ΔG_{Ce}^o were used as the fitting variables for the modeling of the oxygen nonstoichiometry data as a function of P_{O_2} at each temperature.

2. Association model: defect interaction among reduced Pr species and oxygen vacancies is taken into consideration, in addition to the ideal reduction of Pr and Ce (Eq. 3 and 4). The defect interaction is assumed to lead to the formation of a singly charged defect associate, according to

$$Pr_{Ce}' + V_O^{\bullet\bullet} \leftrightarrow (Pr_{Ce}', V_O^{\bullet\bullet})^{\bullet}$$

$$K_{assoc} = \exp\left(-\frac{\Delta H_{assoc}^o - T\Delta S_{assoc}^o}{RT}\right)$$

$$= \frac{[(Pr_{Ce}', V_O^{\bullet\bullet})^{\bullet}]}{[V_O^{\bullet\bullet}][Pr_{Ce}']} \quad \Delta H_{assoc}^o, \ \Delta S_{assoc}^o = \text{const} \quad [9]$$

The mass, site, and charge conservation conditions are modified in this case to

$$[Pr_{Ce}^x] + [Pr_{Ce}'] + [(Pr_{Ce}', V_O^{\bullet\bullet})^{\bullet}] = 0.2 \quad [10]$$

$$[O_O^x] + [V_O^{\bullet\bullet}] + [(Pr_{Ce}', V_O^{\bullet\bullet})^{\bullet}] = 2 \quad [11]$$

$$2[V_O^{\bullet\bullet}] + [(Pr'_{Ce}, V_O^{\bullet\bullet})^{\bullet}] = [Pr'_{Ce}] + [Ce'_{Ce}] \quad [12]$$

Three parameters, ΔG^{o}_{Pr}, ΔG^{o}_{Ce}, and ΔG^{o}_{assoc}, are necessary in this case for the fitting of the experimental data at each temperature.

3. Regular solution model: This model includes the reduction reactions for Pr and Ce, Eq. 3 and 4, with an excess enthalpic term contributing to the reduction of Pr

$$\Delta H^{o}_{Pr} = \Delta H^{o}_{Pr,\delta=0} + \Delta H^{exc}_{Pr} = \Delta H^{o}_{Pr,\delta=0} + 10\delta(1 - 10\delta)\Omega \quad [13]$$

$$0 \leq \delta \leq 0.1$$

where the parameter Ω represents the magnitude of the deviation from the ideal solution and accounts for all the interatomic interactions collectively. $Ce_{0.8}Pr_{0.2}O_{2-\delta}$ is considered to be the solid solution of $Ce_{0.8}Pr_{0.2}O_2$ and $Ce_{0.8}Pr_{0.2}O_{1.9}$ with $x_{Ce_{0.8}Pr_{0.2}O_2} = 1-10\delta$ and $x_{Ce_{0.8}Pr_{0.2}O_{1.9}} = 10\delta$. The equilibrium constant for the reduction of Pr becomes

$$K^{reg}_{Pr} = \exp\left(-\frac{\Delta H^{o}_{Pr,\delta=0} + \Delta H^{exc}_{Pr} - T\Delta S^{o}_{Pr}}{RT}\right) = \frac{P^{1/2}_{O_2}[V_O^{\bullet\bullet}][Pr'_{Ce}]^2}{[O^{x}_{O}][Pr^{x}_{Ce}]^2}$$

$$\Delta H^{o}_{Pr,\delta=0}, \Omega, \Delta S^{o}_{Pr} = \text{const} \quad [14]$$

Five variables ($\Delta H^{o}_{Pr,\delta=0}$, Ω, ΔS^{o}_{Pr}, ΔH^{o}_{Ce}, and ΔS^{o}_{Ce}) were used for the fitting of the oxygen nonstoichiometry data with the regular solution model at all temperatures. The standard enthalpies and entropies used, as well as the parameter Ω, are assumed to be temperature-independent.

4. Nonideal solution model: This model treats the reduction of Pr in a nonideal manner. It includes the reduction reactions for Pr and Ce, Eq. 3 and 4, with an excess enthalpic term, linear with respect to δ, contributing to the reduction of Pr

$$\Delta H^{o}_{Pr} = \Delta H^{o}_{Pr,\delta=0} + \Delta H^{exc}_{Pr} = \Delta H^{o}_{Pr,\delta=0} + a_H\delta \quad [15]$$

where the parameter a_H represents the rate of change in the partial molar enthalpy for the reduction of Pr with oxygen nonstoichiometry $(d\Delta H^{o}_{Pr})/d\delta$. Five variables ($\Delta H^{o}_{Pr,\delta=0}$, a_H, ΔS^{o}_{Pr}, ΔH^{o}_{Ce}, and ΔS^{o}_{Ce}) were used for the fitting of the oxygen nonstoichiometry data with the δ-linear solution model at all temperatures. The standard enthalpies and entropies used, as well as the parameter a_H, are assumed to be temperature-independent.

5. Generalized δ-linear solution model: The reduction of Pr is treated in a nonideal manner by the addition of an excess term to the standard Gibbs energy change

$$\Delta G^{o}_{Pr} = \Delta G^{o}_{Pr,\delta=0} + \Delta G^{exc}_{Pr} = \Delta G^{o}_{Pr,\delta=0} + a_G\delta \quad [16]$$

where the parameter a_G is an indicator of the deviation from the standard Gibbs energy change for the reduction of Pr. This term allows for a linear δ dependency of both the standard enthalpy and entropy change in the reduction of Pr. Three fitting parameters, $\Delta G^{o}_{Pr,\delta=0}$, a_G, and ΔG^{o}_{Ce}, were used in this case at each temperature.

To clarify the behavior of each model, a schematic illustration of the δ dependence of ΔG^{o}_{Pr} for the ideal, regular, δ-linear, and generalized δ-linear solution models at two different temperatures, 600 and 1000°C, is shown in Fig. 4. In the ideal solution model, ΔG^{o}_{Pr} is constant with respect to δ at any temperature, whereas in the regular, δ-linear, and generalized δ-linear solution models, ΔG^{o}_{Pr} varies with δ. In the regular solution model, ΔG^{o}_{Pr} has a temperature-independent, second-order-degree dependency on δ according to $\Delta G^{o}_{Pr} = \Delta H^{o}_{Pr,\delta=0} - T\Delta S^{o}_{Pr} + 10\delta(1 - 10\delta)\Omega$. Its value is identical to that of the ideal model for $\delta = 0$ and $\delta = 0.1$. In the δ-linear solution model, the slope $(d\Delta G^{o}_{Pr})/d\delta$ has the same value at all temperatures, as the excess term is of purely enthalpic origin, whereas in the generalized δ-linear solution model the slope $(d\Delta G^{o}_{Pr})/d\delta$ can vary with temperature, as it comprises an enthalpic and an entropic contribution.

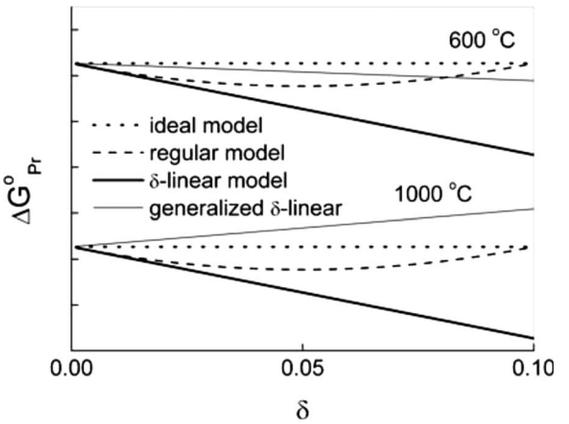

Figure 4. Schematic illustration of the δ dependence of the standard Gibbs energy change, ΔG^{o}_{Pr}, for the ideal, regular, δ-linear, and generalized δ-linear solution models at 600 and 1000°C.

In the fitting of the experimental data, a sequential method[28] was adopted for the nonlinear least-squares fitting procedure in all cases, allowing for the simultaneous contribution of all defect species in the defect equilibrium throughout the entire P_{O_2} range, avoiding the use of Brouwer-type approximations.[29] Absolute values for the oxygen nonstoichiometry were obtained by adjusting the δ value at the minimum slope $(d\Delta\delta)/dP_{O_2}$ of the observed "plateau" to 0.1, corresponding to the complete reduction of Pr. Solving the set of the linear and nonlinear equations for each defect model sequentially yields a prediction for the P_{O_2} of each measured value of δ. Because the δ values close to the plateau suffer a much greater uncertainty in the determination of their corresponding P_{O_2}, the fitting was performed by weighting the square deviation by a factor of $|0.1 - \delta|$ in all cases.

The oxygen nonstoichiometry of $Ce_{0.8}Pr_{0.2}O_{2-\delta}$, measured by CT, TB, and TG as a function of P_{O_2} at temperatures between 600 and 900°C, is shown in Fig. 5a-g, along with the best fit obtained from each of the defect models considered. Good agreement is observed between the oxygen nonstoichiometry values determined by the three different techniques, CT, TB, and TG, validating the accuracy of the data.

For ease of reading the figures, the results of the regular solution model are not depicted, as they practically coincide with the results of the ideal and association models. Their predictions significantly deviate from the measured values of δ for the oxygen nonstoichiometry regime corresponding to the reduction of Pr($\delta < 0.1$), at temperatures between 600 and 700°C. A magnification of this regime is shown as insets in Fig. 5a-c, where the failure of the ideal association (and regular) solution models to describe the experimental data can be clearly observed. The measured oxygen nonstoichiometry has a greater dependence on P_{O_2} than predicted by these models. Both the δ-linear and generalized δ-linear solution models are able to accurately reproduce the P_{O_2} dependency of δ over the entire P_{O_2} range examined at each temperature. The deviation between the measured nonstoichiometry data and the ideal association (or regular) model predictions decreases with increasing temperature, as shown in Fig. 5a-g. This is also evidenced by the convergence of the χ^2 values, arising from the fitting with the various defect models, above 750°C, as shown in Fig. 5h. Above this temperature, all five models describe the nonstoichiometry data well. This is due to the much smaller δ range covered at higher temperatures in the regime corresponding to the reduction of Pr. A temperature dependence of the nonideality terms, ΔH^{exc}_{Pr} and ΔS^{exc}_{Pr}, which

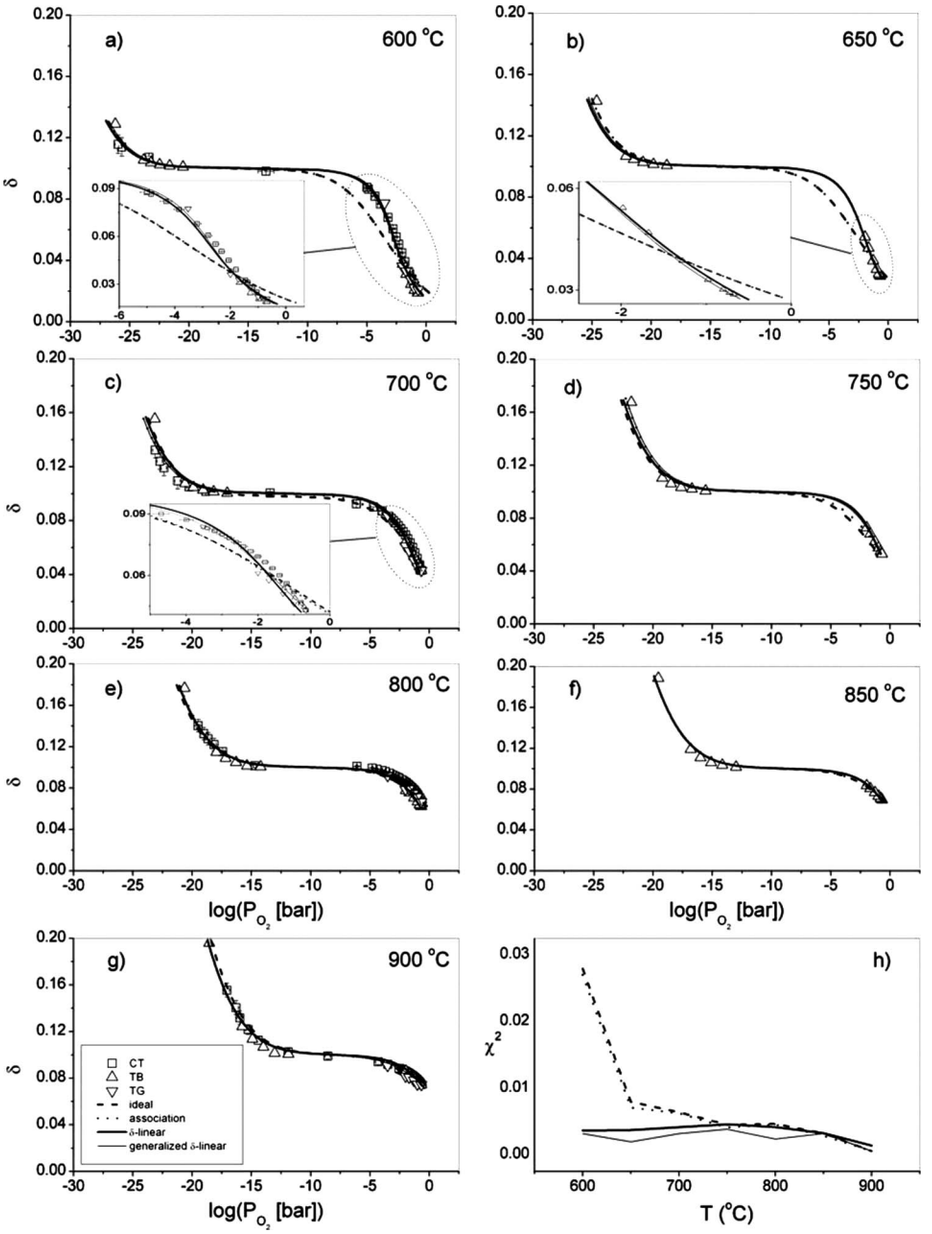

Figure 5. Fit of the various defect models to the oxygen nonstoichiometry data of $Ce_{0.8}Pr_{0.2}O_{2-\delta}$ at (a) 600, (b) 650, (c) 700, (d) 750, (e) 800, (f) 850, and (g) 900°C and (h) comparison of the agreement factor χ^2 obtained from each defect model as a function of temperature.

either has been neglected (δ-linear solution model) or has not been taken explicitly into account (generalized δ-linear solution model), could also play a role.

At temperatures above 750°C, the oxygen nonstoichiometry is well described by an ideal model consistent with the behavior reported in Ref. 19. Another study[20] performed at lower temperatures, 600–750°C, at the P_{O_2} range between 10^{-5} and 10^{-1} atm suggested ideal behavior. However, the examined powder was nanosized, which significantly alters the reduction properties.[26,27]

The reduction of Ce was modeled in an ideal manner, i.e., ΔH^{o}_{Ce}, ΔS^{o}_{Ce} = const, in all cases. Nevertheless, the $\delta(\log P_{O_2})$ behavior estimated from the various defect models, in the oxygen nonstoichiometry regime corresponding to the reduction of Ce($\delta > 0.1$), overall, agrees well with the experimentally determined values. The measured $\delta(\log P_{O_2})$ values in this regime indicate a larger $d\delta/(d \log P_{O_2})$ slope than that predicted from the ideal solution model for the reduction of Ce in all cases, especially at temperatures below 750°C. The limited oxygen nonstoichiometry range covered at low temperatures in this regime does not allow conclusion on whether the reduction of Ce takes place in a nonideal manner. The extended oxygen nonstoichiometry range covered for $\delta > 0.1$ at high temperatures indicates ideal behavior. However, this observation is not adequate to conclude ideal behavior because it could arise from a temperature dependence of the nonideality parameters. The reduction behavior of $Ce_{0.8}Pr_{0.2}O_{2-\delta}$ for $\delta > 0.1$ bears a close similarity to that of $CeO_{2-\delta}$ [5,6] and $Ce_{0.8}Gd_{0.2}O_{1.9-\delta}$ [8] at a total vacancy concentration above 0.1, namely, a small or almost negligible δ dependence of the partial molar enthalpy for oxidation.

The change in the Gibbs energy of formation of $Ce_{0.8}Pr_{0.2}O_{2-\delta}$ relative to $Ce_{0.8}Pr_{0.2}O_{1.9}$ can be estimated from

$$\Delta G_f = \int_{0.1}^{\delta} [\mu_O(\delta) - \mu^{o}_{O}] d\delta = \frac{RT}{2} \int_{0.1}^{\delta} \ln P_{O_2}(\delta) d\delta \qquad [17]$$

R being the universal gas constant. A comparison between the change in the Gibbs energy of formation directly obtained from the

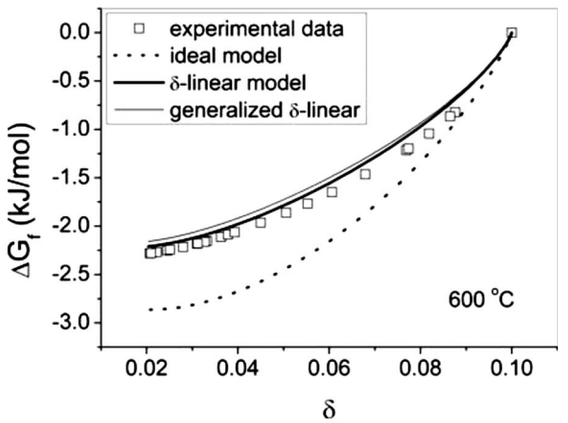

Figure 6. Comparison of the change in the Gibbs energy of formation ΔG_f obtained directly from the nonstoichiometry data with those estimated from the various defect models at 600°C.

nonstoichiometry data and the one estimated from the various defect models has been suggested[13] to be more appropriate than a comparison of the measured and fitted $\delta(\log P_{O_2})$ curves when trying to compare the success of the different defect models. For $SrFeO_{3-\delta}$, although an ideal model appeared more successful in reproducing the $\delta(\log P_{O_2})$ curve for δ smaller than ~0.2, when comparing the Gibbs energy of formation as a function of δ, the regular solution model gave the best agreement.[13] A comparison of ΔG_f directly obtained from the nonstoichiometry data with those estimated from the ideal, δ-linear, and generalized δ-linear solution models for the oxygen nonstoichiometry regime corresponding to the reduction of Pr is shown in Fig. 6 for $T = 600$°C. Very good agreement is observed between the change in the Gibbs energy of formation obtained directly from the nonstoichiometry data and those estimated from the δ-linear and generalized δ-linear solution models throughout the entire oxygen nonstoichiometry range examined. The value estimated from the ideal model significantly deviates. The association and regular solution models are not discussed further as they yield results very similar to the ideal one.

The partial molar enthalpy and entropy for oxygen incorporation were determined from the nonstoichiometry data using the relations

$$h_O(\delta) - h_O^o = \left. \frac{R}{2} \frac{d \ln P_{O_2}}{d(1/T)} \right|_\delta \quad [18]$$

$$s_O(\delta) - s_O^o = - \left. \frac{R}{2} \frac{d(T \ln P_{O_2})}{dT} \right|_\delta \quad [19]$$

Values of P_{O_2}, corresponding to the same amount of δ at different temperatures, were obtained by a linear interpolation of the experimental data. The partial molar quantities were only estimated for values of δ, where P_{O_2} values for at least four temperatures could be used, as this is expected to increase the accuracy of the determined partial molar quantities from Eq. 18 and 19.

Values for $h_O - h_O^o$ and $s_O - s_O^o$ may also be estimated from the fitting parameters and defect concentrations obtained from the various defect models using expressions derived from a statistical thermodynamic analysis (see the Appendix)

$$h_O(\delta) - h_O^o = - \Delta H_{Ce}^o + \frac{\partial [Pr'_{Ce}]}{\partial \delta} \left(\frac{\Delta H_{Ce}^o - \Delta H_{Pr}^o - \Delta H_{Pr}^{exc}}{2} \right) \quad [20]$$

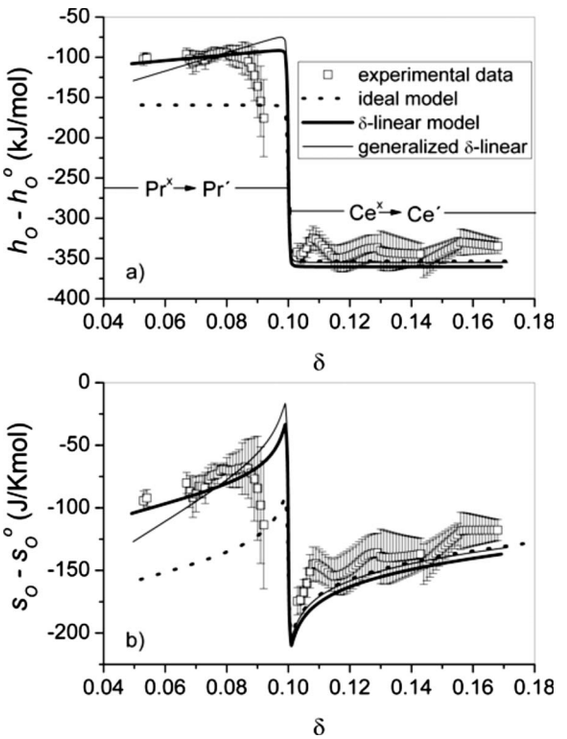

Figure 7. (a) Partial molar enthalpy $h_O - h_O^o$ and (b) entropy $s_O - s_O^o$ for oxygen incorporation as a function of δ for $Ce_{0.8}Pr_{0.2}O_{2-\delta}$.

$$s_O(\delta) - s_O^o = - \Delta S_{Ce}^o + \frac{\partial [Pr'_{Ce}]}{\partial \delta} \left(\frac{\Delta S_{Ce}^o - \Delta S_{Pr}^o - \Delta S_{Pr}^{exc}}{2} \right) + s_O^{conf} \quad [21]$$

where s_O^{conf} is the configurational part of the partial molar entropy of oxidation of $Ce_{0.8}Pr_{0.2}O_{2-\delta}$ given from Eq. A-11, and the partial derivative of the concentration of Pr'_{Ce} with respect to δ is given as a function of the equilibrium constants of Reactions 3 and 4 and the defect concentrations from Eq. A-12. In the P_{O_2} range, where the change in oxygen nonstoichiometry is related to reduction of Pr, i.e., when $[Pr'_{Ce}] \approx 2\delta$, Eq. 20 and 21 become

$$h_O(\delta) - h_O^o \approx - \Delta H_{Pr}^o - \Delta H_{Pr}^{exc} \quad [22]$$

$$s_O(\delta) - s_O^o \approx - \Delta S_{Pr}^o - \Delta S_{Pr}^{exc} + R \ln \left(\frac{[V_O^{\bullet\bullet}][Pr'_{Ce}]^2}{[O_O^x][Pr_{Ce}^x]^2} \right) \quad [23]$$

whereas in the P_{O_2} range where the change in oxygen nonstoichiometry is related to the reduction of Ce, i.e., when $[Ce'_{Ce}] \approx 2\delta - 0.2$, we obtain

$$h_O(\delta) - h_O^o \approx - \Delta H_{Ce}^o \quad [24]$$

$$s_O(\delta) - s_O^o \approx - \Delta S_{Ce}^o + R \ln \left(\frac{[V_O^{\bullet\bullet}][Ce'_{Ce}]^2}{[O_O^x][Ce_{Ce}^x]^2} \right) \quad [25]$$

The δ dependency of the partial molar enthalpy and entropy, as directly determined from the nonstoichiometry data, is shown in Fig. 7a and b, respectively, and compared with the values estimated from the various defect models. The values of $h_O - h_O^o$ and $s_O - s_O^o$ estimated from the δ-linear and generalized δ-linear solution models agree with those directly determined from the oxygen nonstoichiometry data using Eq. 18 and 19. The values of $h_O - h_O^o$ and $s_O - s_O^o$ estimated from the ideal model are significantly underestimated in the nonstoichiometry range related to the reduction of Pr($\delta < 0.1$).

The generalized δ-linear solution model yields larger values for the slopes $[d(h_O - h_O^o)]/d\delta$ and $[d(s_O - s_O^o)]/d\delta$ than the values directly determined from the nonstoichiometry data for $\delta < 0.1$, whereas the δ dependency of $h_O - h_O^o$ and $s_O - s_O^o$ estimated from the δ-linear solution model agrees very well with the one directly determined from the oxygen nonstoichiometry data over the entire δ range examined. The observed nonideality in the reduction of Pr should therefore be attributed to a change in the enthalpy for oxygen incorporation with varying oxygen nonstoichiometry.

According to the definition of the ideal, regular, and δ-linear solution models, the value of $h_O - h_O^o$ should be identical at $\delta = 0$ in all three cases. Also, the δ dependence of $s_O - s_O^o$ should be identical because there is no excess entropic term present in any of these models, and a random distribution of defects is assumed in all cases. None of these conditions is true though when comparing the $h_O - h_O^o$ and $s_O - s_O^o$ values for the ideal and δ-linear solution models in Fig. 7a and b. This is because $\Delta H^o_{Pr,\delta=0}$ and ΔS^o_{Pr} were not constrained to have the same values in all defect models but instead were allowed to vary freely in each defect model. Because each defect model has a different number and type of fitting parameters, the best fit in each case is not expected to result in the same $\Delta H^o_{Pr,\delta=0}$ and ΔS^o_{Pr} values.

The negative sign of $h_O - h_O^o$ indicates that the incorporation of oxygen is an exothermic process. The value of $h_O - h_O^o$ for $\delta < 0.1$ is related to the oxidation of Pr and varies between −103 and −93 kJ/mol in the nonstoichiometry range between 0.053 and 0.08. A value of -73 ± 6 kJ/mol has been reported[19] for the partial molar enthalpy for the oxidation of Pr in $Ce_{0.8}Pr_{0.2}O_{2-\delta}$ from the nonstoichiometry data obtained in the temperature range of 800–950°C after fitting with an ideal defect model. The value of $h_O - h_O^o$ increases with increasing δ, indicating a more facilitated expulsion of oxygen with increasing fractional concentration of trivalent Pr. A similar behavior has been observed for the reduction of Ce in $CeO_{2-\delta}$ [5,6] and $Ce_{0.9}Gd_{0.1}O_{1.95-\delta}$ [7] at a similar total oxygen vacancy concentration range. This is probably related to the decrease in the strength of the metal–oxygen bond with decreasing valency and increasing ionic radii of the cations. This possibility is discussed in more detail later on. A sharp decrease in the value of $h_O - h_O^o$ is observed in the nonstoichiometry range between 0.08 and 0.09. This is attributed to increased uncertainty in this region, arising from increased experimental errors, errors in the shifting of the $\Delta\delta(\log P_{O_2})$ curves to obtain absolute values of δ, as well as increased errors entering the analysis due to the sparser data points in this region.

In the oxygen nonstoichiometry range $\delta > 0.1$, where the incorporation of oxygen is related to the oxidation of Ce, the values of $h_O - h_O^o$ and $s_O - s_O^o$ estimated from the various models are slightly underestimated relative to the values obtained directly from the oxygen nonstoichiometry data. A mean value of $h_O - h_O^o$ of -340 ± 7 kJ/mol is obtained from the experimental data in the δ range between 0.103 and 0.168, whereas values between −353 and −359 kJ/mol are estimated from various defect models. This indicates that a nonideal solution model might be more appropriate for the modeling of the reduction of Ce as well, but the limited amount of data in this region does not allow for a definite conclusion. The reduction of Ce was modeled in an ideal manner, i.e., ΔH^o_{Ce}, ΔS^o_{Ce} = const, in all cases. The small differences observed in the values of $h_O - h_O^o$ and $s_O - s_O^o$ estimated from the various models in this region are a result of the influence of the way the reduction of Pr was treated and of uncertainties arising from the fitting.

The values of the nonideality parameters, a_H and a_G, obtained from the fit of the δ-linear and generalized δ-linear solution models to the $\delta(\log P_{O_2})$ curves at temperatures between 600 and 850°C, are shown in Fig. 8. A constant value of -354 ± 1 kJ/mol^2 was determined for a_H from the fitting of the $\delta(\log P_{O_2})$ curves at all temperatures (it is assumed to be temperature-independent). The values obtained for a_G from the fitting of the $\delta(\log P_{O_2})$ curves at each

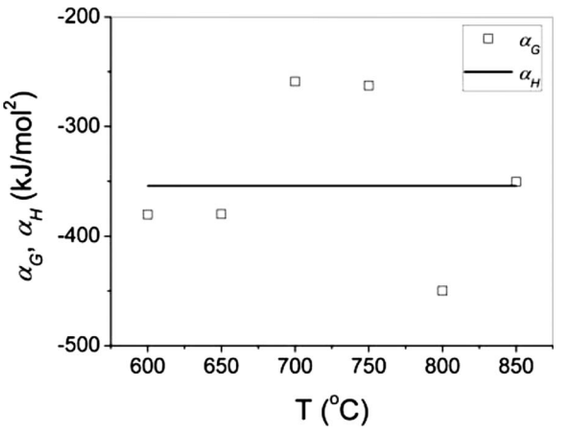

Figure 8. Nonideality parameters, a_H and a_G, as a function of temperature.

temperature show considerable scattering without indicating a certain temperature dependence. The mean value of a_G in this temperature range is -350 ± 70 kJ/mol^2, agreeing with the value determined for a_H from the δ-linear solution model within experimental uncertainty. The temperature independence of a_G indicates the lack of an excess entropic term for the nonideal reduction behavior of Pr. The negative value of a_H causes an increase in $h_O - h_O^o$ with increasing oxygen nonstoichiometry (Eq. 15 and 20), which results in a facilitated expulsion of oxygen with increasing δ. The value of a_H or a_G estimated here for $Ce_{0.8}Pr_{0.2}O_{2-\delta}$ is of the same magnitude as found for perovskite systems.[12,30] The value of a_G varies between −400 and −250 kJ/mol^2 for $La_{1-x}Ca_xCrO_{3-\delta}$, depending on x and temperature,[12] whereas the value of a_H varied between −600 and −100 kJ/mol^2 for $La_{0.9}Ca_{0.1}Cr_{1-y}Al_yO_{3-\delta}$, depending on y. [30]

A linear relationship between the excess Gibbs free energy and the oxygen nonstoichiometry was confirmed in $La_{1-x}Ca_xCrO_{3-\delta}$ [12] on the basis of changes in the interatomic potentials due to the defect induced volumetric expansion. A similar approach is undertaken here, describing the interatomic interactions by a Buckingham-type shell-model potential[31]

$$U_{ij} = A_{ij} \exp\left(-\frac{r_{ij}}{\rho_{ij}}\right) - \frac{C_{ij}}{r_{ij}^6} \qquad [26]$$

where A_{ij}, ρ_{ij}, and C_{ij} are constants characteristic of the pair i–j and r_{ij} is the distance between ions i and j. A_{ij}, ρ_{ij}, and C_{ij} values refined for ceria were used,[32] and the interatomic distances r_{ij} were determined by Rietveld refinement of the room-temperature XRD pattern of $Ce_{0.8}Pr_{0.2}O_2$ and values of the deconvoluted thermal and chemical expansion coefficients,[33] $a_{int}(30–600°C) = 11.3 \times 10^{-6}$ K^{-1}, $a_{int}(30–800°C) = 12.6 \times 10^{-6}$ K^{-1}, and $\beta = 0.084$ mol^{-1}, assuming isotropic expansion of all interatomic distances. The excess enthalpy may then be estimated from

$$\Delta H^{exc}_{Pr} = \sum_{i,j\neq i} \Delta U_{ij} = \sum_{i,j\neq i} [U_{ij}(r_{ij} + \Delta r_{ij}) - U_{ij}(r_{ij})] \qquad [27]$$

where $\Delta r_{ij} = \beta\delta r_{ij}$ is the defect induced (chemical) expansion of the interatomic distance r_{ij}. The summation of the pair potentials in Eq. 27 was restricted to the first neighbors only in this simplistic calculation. The estimated dependence of the excess enthalpic term on oxygen nonstoichiometry at 600°C is shown in Fig. 9.

As shown in Fig. 9, the estimated excess enthalpy is far from zero that would be required for an ideal solution behavior. Furthermore, an almost linear relationship between excess enthalpy and δ can be observed from Fig. 9, with a slope of −332 kJ/mol^2, which agrees semiquantitatively with the experimentally determined value of -354 ± 1 kJ/mol^2 for a_H. A value of −328 kJ/mol^2 would be calculated at 800°C, indicating no temperature dependence of the

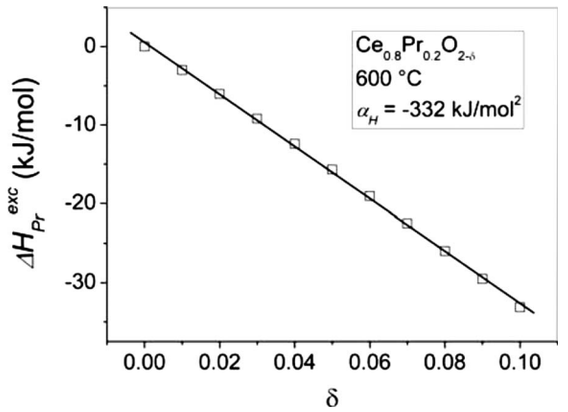

Figure 9. Excess enthalpy as a function of oxygen nonstoichiometry. The straight line is the result of linear fitting, yielding a slope $\alpha_H = -332$ kJ/mol^2.

nonideality parameter. This calculation is in support of the δ-linear solution model that was able to describe the experimentally determined nonstoichiometry data, while at the same time it suggests a decrease in the mean metal–oxygen bond strength to be the reason for the observed nonideal behavior of the reduction of Pr in $Ce_{0.8}Pr_{0.2}O_{2-\delta}$.

Conclusion

The oxygen nonstoichiometry of $Ce_{0.8}Pr_{0.2}O_{2-\delta}$ was measured by CT and TG over a wide P_{O_2} range, covering both the reduction of Pr and Ce at temperatures between 600 and 900°C. Five defect models were applied to the nonstoichiometry data. The reduction of Pr could not be modeled in an ideal manner (constant ΔH^o_{Pr} and ΔS^o_{Pr}) even with an additional defect reaction taking into account the association of reduced Pr species and oxygen vacancies. A regular solution model was also unable to explain the P_{O_2} dependence of the oxygen nonstoichiometry. A nonideal solution model with a linear δ dependence of ΔH^o_{Pr} (δ-linear) and a nonideal solution model with a linear δ dependence of ΔG^o_{Pr} (generalized δ-linear) for the reduction of Pr could accurately reproduce the $\delta(\log\ P_{O_2})$ curves in the entire nonstoichiometry range examined and at all temperatures, at the same time yielding a δ dependence of ΔG_f, which agrees very well with the one directly determined from the nonstoichiometry data. The partial molar enthalpy and entropy of oxidation estimated from the ideal model were significantly underestimated relative to the values obtained directly from the nonstoichiometry data, whereas the δ-linear solution model yielded a very good agreement. This indicates that the observed nonideal behavior of the reduction of Pr is due to a δ-dependent $h_O - h^o_O$ giving rise to a facilitated loss of oxygen with increasing fractional concentration of trivalent Pr. This is tentatively attributed to a decrease in the strength of the metal–oxygen bond with decreasing oxidation state and increasing ionic radii of Pr.

Acknowledgments

Financial support from the Danish Council for Strategic Research, Programme Commission on Sustainable Energy and Environment, project no. 2104-0450041 is gratefully acknowledged.

Risø DTU, National Laboratory for Sustainable Energy assisted in meeting the publication costs of this article.

Appendix

The standard Gibbs free energy change in Reactions 3 and 4 may be expressed as a function of the standard chemical potential of the quasi-chemical species involved as

$$\Delta G^o_{Pr} = 2\mu^o_{Pr'_{Ce}} + \mu^o_{V^{\bullet\bullet}_O} + \tfrac{1}{2}\mu^o_{O_2,gas} - 2\mu^o_{Pr^x_{Ce}} - \mu^o_{O^x_O} \quad [A\text{-}1]$$

$$\Delta G^o_{Ce} = 2\mu^o_{Ce'_{Ce}} + \mu^o_{V^{\bullet\bullet}_O} + \tfrac{1}{2}\mu^o_{O_2,gas} - 2\mu^o_{Ce^x_{Ce}} - \mu^o_{O^x_O} \quad [A\text{-}2]$$

The Gibbs free energy of $Ce_{0.8}Pr_{0.2}O_{2-\delta}$ is

$$G = \sum_i x_i\mu_i = \sum_i x_i\mu^o_i + RT\sum_i x_i\ \ln\ \gamma_i x_i \quad [A\text{-}3]$$

The chemical potential of oxygen of $Ce_{0.8}Pr_{0.2}O_{2-\delta}$ relative to that of the standard state can be estimated from

$$\mu_O - \mu^o_O = \frac{\partial G}{\partial (2-\delta)} - \mu^o_O = -\sum_i \mu^o_i \frac{\partial x_i}{\partial \delta} - \mu^o_O - RT\frac{\partial}{\partial \delta}\sum_i x_i\ \ln\ x_i - RT\sum_i \ln\ \gamma_i \frac{\partial x_i}{\partial \delta} \quad [A\text{-}4]$$

The combination and differentiation of the mass, site, and charge conservation conditions, Eq. 5-8, yield

$$\frac{\partial [Pr^x_{Ce}]}{\partial \delta} = -\frac{\partial [Pr'_{Ce}]}{\partial \delta} \quad [A\text{-}5]$$

$$\frac{\partial [Ce^x_{Ce}]}{\partial \delta} = -\frac{\partial [Ce'_{Ce}]}{\partial \delta} \quad [A\text{-}6]$$

$$\frac{\partial [O^x_O]}{\partial \delta} = -\frac{\partial [V^{\bullet\bullet}_O]}{\partial \delta} = -1 \quad [A\text{-}7]$$

$$\frac{\partial [Ce'_{Ce}]}{\partial \delta} = 2 - \frac{\partial [Pr'_{Ce}]}{\partial \delta} \quad [A\text{-}8]$$

The configurational entropy of $Ce_{0.8}Pr_{0.2}O_{2-\delta}$ is

$$S^{conf} = k\left[\ln\left(\frac{(2N_A)!}{([V^{\bullet\bullet}_O]N_A)!\,[(2-[V^{\bullet\bullet}_O])N_A]!}\right) + \ln\left(\frac{(0.2N_A)!}{([Pr'_{Ce}]N_A)!\,([Pr^x_{Ce}]N_A)!}\right) + \ln\left(\frac{(0.8N_A)!}{([Ce'_{Ce}]N_A)!\,([Ce^x_{Ce}]N_A)!}\right) + \ln\left(\frac{N_A!}{(0.2N_A)!\,(0.8N_A)!}\right)\right] \quad [A\text{-}9]$$

where k is Boltzmann's constant. The configurational part of the partial molar entropy of oxidation of $Ce_{0.8}Pr_{0.2}O_{2-\delta}$ is then estimated from

$$s^{conf}_O = \frac{\partial S^{conf}}{\partial (2-\delta)} = -\frac{\partial S^{conf}}{\partial \delta} \quad [A\text{-}10]$$

Substituting $R = kN_A$ and Eq. A-5-A-9 in Eq. A-10 yields

$$s^{conf}_O = R\left[\ln\left(\frac{(2\delta - [Pr'_{Ce}])^2\delta}{(0.8-2\delta+[Pr'_{Ce}])^2(2-\delta)}\right) + \frac{\partial [Pr'_{Ce}]}{\partial \delta}\ln\left(\frac{[Pr'_{Ce}](0.8-2\delta+[Pr'_{Ce}])}{(0.2-[Pr'_{Ce}])(2\delta-[Pr'_{Ce}])}\right)\right] \quad [A\text{-}11]$$

Dividing Eq. 3 and 4, differentiating with respect to δ, and solving for the partial derivative of the concentration of Pr'_{Ce} with respect to δ, we obtain

$$\frac{\partial [Pr'_{Ce}]}{\partial \delta} = \frac{4K_{Pr}[Ce'_{Ce}][Pr^x_{Ce}]^2 + 4K_{Ce}[Ce^x_{Ce}][Pr'_{Ce}]^2}{2K_{Ce}([Pr'_{Ce}][Ce^x_{Ce}]^2 + [Ce^x_{Ce}][Pr'_{Ce}]^2) + 2K_{Pr}([Pr^x_{Ce}][Ce'_{Ce}]^2 + [Ce'_{Ce}][Pr^x_{Ce}]^2)} \quad [A\text{-}12]$$

Substituting Eq. A-1, A-2, A-5-A-8, and A-11 in Eq. A-4, and separating the enthalpic from the entropic contribution, we obtain

$$h_O(\delta) - h^o_O = -\Delta H^o_{Ce} + \frac{\partial [Pr'_{Ce}]}{\partial \delta}\left(\frac{\Delta H^o_{Ce} - \Delta H^o_{Pr} - \Delta H^{exc}_{Pr}}{2}\right) \quad [A\text{-}13]$$

$$s_O(\delta) - s^o_O = -\Delta S^o_{Ce} + \frac{\partial [Pr'_{Ce}]}{\partial \delta}\left(\frac{\Delta S^o_{Ce} - \Delta S^o_{Pr} - \Delta S^{exc}_{Pr}}{2}\right) + s^{conf}_O \quad [A\text{-}14]$$

References

1. B. C. H. Steele, *Solid State Ionics*, **134**, 3 (2000).
2. A. Trovarelli, *Catal. Rev. - Sci. Eng.*, **38**, 439 (1996).
3. O. Yamamoto, in *Solid State Electrochemistry*, P. G. Bruce, Editor, p. 292, Cambridge University Press, Cambridge, MA (1995).
4. M. Stoukides, *Catal. Rev. - Sci. Eng.*, **42**, 1 (2000).
5. D. J. M. Bevan and J. Kordis, *J. Inorg. Nucl. Chem.*, **26**, 1509 (1964).
6. R. J. Panlener, R. N. Blumenthal, and J. E. Garnier, *J. Phys. Chem. Solids*, **36**, 1213 (1975).
7. S. Wang, H. Inaba, H. Tagawa, M. Dokiya, and T. Hashimoto, *Solid State Ionics*, **107**, 73 (1998).
8. S. Wang, H. Inaba, H. Tagawa, and T. Hashimoto, *J. Electrochem. Soc.*, **144**, 4076 (1997).
9. M. Mogensen, in *Catalysis by Ceria and Related Materials*, A. Trovarelli, Editor, pp. 453–481, Imperial College Press, London (2002).

10. J. Mizusaki, S. Yamauchi, K. Fueki, and A. Ishikawa, *Solid State Ionics*, **12**, 119 (1984).
11. J. Mizusaki, Y. Mima, S. Yamauchi, K. Fueki, and H. Tagawa, *J. Solid State Chem.*, **80**, 102 (1989).
12. S. Onuma, K. Yashiro, S. Miyoshi, A. Kaimai, H. Matsumoto, Y. Nigara, T. Kawada, J. Mizusaki, K. Kawamura, N. Sakai, et al., *Solid State Ionics*, **174**, 287 (2004).
13. E. Bakken, S. Stølen, T. Norby, R. Glenne, and M. Budd, *Solid State Ionics*, **167**, 367 (2004).
14. P. Shuk and M. Greenblatt, *Solid State Ionics*, **116**, 217 (1999).
15. C. Ftikos, M. Nauer, and B. C. H. Steele, *J. Eur. Ceram. Soc.*, **12**, 267 (1993).
16. M. Y. Sinev, G. W. Graham, L. P. Haack, and M. Shelef, *J. Mater. Res.*, **11**, 1960 (1996).
17. P. Knauth and H. L. Tuller, *J. Eur. Ceram. Soc.*, **19**, 831 (1999).
18. M. Rajendran, K. K. Mallick, and A. K. Bhattacharya, *J. Mater. Sci.*, **33**, 5001 (1998).
19. D. P. Fagg, I. P. Marozau, A. L. Shaula, V. V. Kharton, and J. R. Frade, *J. Solid State Chem.*, **179**, 3347 (2006).
20. T. S. Stefanik and H. L. Tuller, *J. Electroceram.*, **13**, 799 (2004).
21. A. B. Koudriavtsev, R. F. Jameson, and W. Linert, *The Law of Mass Action*, p. 204, Springer-Verlag, New York (2001).
22. J. Mizusaki, H. Tagawa, K. Naraya, and T. Sasamoto, *Solid State Ionics*, **49**, 111 (1991).
23. V. A. Cherepanov, L. Y. Barkhatova, and V. I. Voronin, *J. Solid State Chem.*, **134**, 38 (1997).
24. K. Yashiro, S. Onuma, A. Kaimai, Y. Nigara, T. Kawada, J. Mizusaki, K. Kawamura, T. Horita, and H. Yokokawa, *Solid State Ionics*, **152–153**, 469 (2002).
25. M. Katsuki, S. Wang, K. Yasumoto, and M. Dokiya, *Solid State Ionics*, **154–155**, 589 (2002).
26. T. Kobayashi, S. Wang, M. Dokiya, H. Tagawa, and T. Hashimoto, *Solid State Ionics*, **126**, 349 (1999).
27. Y. M. Chiang, E. B. Lavik, and D. A. Blom, *Nanostructured Materials*, **9**, 633 (1997).
28. F. W. Poulsen, in *Proceedings of Nordic Workshop on High Temperature Electrode Materials*, Risø National Laboratory for Sustainable Energy, Roskilde, Denmark (1992).
29. G. Brouwer, *Philips Res. Rep.*, **9**, 366 (1954).
30. J. Mizusaki, M. Hasegawa, K. Yashiro, H. Matsumoto, and T. Kawada, *Solid State Ionics*, **177**, 1925 (2006).
31. B. Dick and A. Overhauser, *Phys. Rev.*, **112**, 90 (1958).
32. A. Gotte, D. Spångberg, K. Hermansson, and M. Baudin, *Solid State Ionics*, **178**, 1421 (2007).
33. C. Chatzichristodoulou, P. V. Hendriksen, and A. Hagen, *J. Electrochem. Soc.*, **157**, B299 (2010).